Overcoming Unknown Measurement Noise Powers in Multistatic Target Localization: A Cyclic Minimization and Joint Estimation Algorithm

Jing YANG, Chengcheng LIU, Jie HUANG, Dexiu HU, Chuang ZHAO

National Digital Switching System Engineering and Technological Research Center, Zhengzhou 450000, China

yangjing1028@126.com, luckylcc079@126.com, huangjie0922@126.com, skylar1235@126.com, rushzhao@163.com

Submitted March 5, 2023 / Accepted June 29, 2023 / Online first August 7, 2023

Abstract. *This paper investigates the issue of multistatic target localization using measurements including angle of arrival (AOA), time delay (TD), and Doppler shift (DS). We delve into a practically driven nonideal localization scenario where the measurement noise powers remain unknown. An algorithm that jointly estimates target position-velocity and measurement noise powers is proposed. Initially, an optimization model for the joint estimation is developed following the maximum likelihood estimation criterion. Subsequently, we cyclically minimize the optimization model to yield estimates for target position-velocity and measurement noise powers. The Cramér-Rao lower bound (CRLB) for this joint estimation is also derived. Contrary to existing algorithms, our proposed method eliminates the need for prior knowledge of measurement noise powers, simultaneously estimating the target position-velocity and measurement noise powers. Simulation results indicate superior localization accuracy with our algorithm, particularly in scenarios with unknown measurement noise powers. Furthermore, at moderate noise levels, the algorithm's estimation accuracy for target position-velocity and measurement noise powers meets the CRLB.*

Keywords

Multistatic target localization, angle of arrival, time delay, Doppler shift, measurement noise power

1. Introduction

Multistatic target localization techniques find extensive applications in various areas such as wireless sensor networks, multiple-input multiple-output (MIMO) radar, multistatic passive radar, navigation, atmospheric monitoring, ionospheric studies, and multi-antenna systems [1–4]. These systems leverage multiple transmitters and receivers to detect and pinpoint potential targets. The potential for enhanced resolution, resilience against channel fading and interference interception, and overall improvement in target localization has led to increased academic interest in this field over recent years.

The commonly employed measurements in multistatic target localization are time delay (TD), Doppler shift (DS), and angle of arrival (AOA) of the target echo signal at the receivers. For target position estimation, some studies utilize TD information as the measurement, and presents some effective localization algorithms such as the singular value decomposition (SVD) algorithm in [5], the two stage weighted least squares (2WLS) algorithm in [6], the convex optimization in [7], the majorization-minimization in [8], to estimate the target position. When the receiver has goniometric capability, TD and AOA measurements can be jointly used to enhance localization accuracy, such as the 2WLS solution in [9], the one stage weighted least squares (1WLS) solution in [10], [11], quadratic constraint [12], and the convex solution in [13]. For the position and velocity estimation of moving targets, DS measurement can also be used in addition to TD measurement to estimate accurately the target position and velocity, such as the iterative Lagrange programming neural network based algorithm in [14], the TSWLS and its variants in [15–19]. However, the above mentioned studies employ either one (TD-based localization [5–8]) or two (hybrid TD-AOA localization [9–13], hybrid TD-DS localization [14–19]) of the TD, DS and AOA measurements for target location. The hybrid TD-DS-AOA localization method, which uses all three types of measurements, offers theoretically higher localization accuracy and robustness by providing estimates for both target position and velocity. Consequently, to further improve the performance of multistatic localization systems, there has been growing interest in TD-DS-AOA-based multistatic target localization, and some effective algorithms have been developed.

Li et al. [21] categorized TD-DS-AOA measurements into distinct groups based on different receivers, employing the classic multi-stage weighted least squares (mWLS) approach [22] to generate a target position and velocity estimate from each measurement group. The final estimate of the target position and velocity was then obtained by merging these group estimates through linear weighted

DOI: 10.13164/re.2023.0415

least squares. However, Li et al.'s algorithm assumes that measurement noises in different groups are independent, an assumption that often fails in practice and can lead to diminished localization performance. Alternatively, Yang et al. [23] proposed an mWLS-based localization algorithm without such grouping. They transformed the TD-DS-AOA measurement equations into pseudo-linear matrix equations by introducing multiple auxiliary variables simultaneously. Then, they used the mWLS processing to extract the target position and velocity estimate from these equations. While Yang et al.'s algorithm is theoretically and numerically shown to achieve the estimation accuracy of the Cramér-Rao lower bound (CRLB) at sufficiently small measurement noise levels, the multi-stage processing can lead to error propagation between stages, making the algorithm sensitive to measurement noises. To address this issue, Wei et al. [24] combined the AOA measurements with TD and DS measurement equations and linearized the TD-DS-AOA measurement equations without introducing any auxiliary variables. In contrast to the frequently used mWLS estimators, Wei et al.'s algorithm estimates the target position and velocity using only a single-stage WLS minimization, thereby avoiding interstage error propagation. However, these existing algorithms rely on prior knowledge of the measurement noise powers, which is not always feasible in practical scenarios. Therefore, there is an urgent need to develop a localization algorithm that does not require prior knowledge of the measurement noise powers.

Motivated by these considerations, our investigation extends to multistatic target localization using TD-DS-AOA measurements. The main contributions of this work include:

(a) A multistatic localization system with multiple transmitters and multiple receivers is considered, but unlike previous studies, the measurement noise powers are assumed unknown, which is closer to the actual non-ideal scenario.

(b) We propose an estimator that jointly determines target position-velocity and measurement noise powers. Firstly, a joint optimization model for target position-velocity and measurement noise powers is deduced based on the maximum likelihood estimation (MLE) criterion. To counter the nonconvexity and nonlinearity of the optimization model, we apply a cyclical minimization optimization strategy to obtain the target position-velocity and measurement noise power estimates.

(c) CRLB analysis and numerical simulations are conducted to validate the effectiveness and superiority of our proposed algorithm.

This paper is organized into six sections. Section 2 formulates the problem of multistatic target localization. Section 3 presents our proposed localization algorithm. In Sec. 4, we derive the CRLB for the joint estimation of target localization and measurement noise powers. Section 5 involves numerical simulations to evaluate the performance of our proposed algorithm. Finally, conclusions are drawn in Sec. 6.

2. Problem Formulation

In the scenario depicted in Fig. 1, we consider a multistatic localization system comprising N_t transmitters and N_r receivers, aimed at locating moving targets within a three-dimensional (3-D) space. For the ith transmitter and the jth receiver, their respective positions are symbolized as $\mathbf{s}_{t,i}=[x_{t,i}, y_{t,i}, z_{t,i}]^T$ and $\mathbf{s}_{r,i}=[x_{r,i}, y_{r,i}, z_{r,i}]^T$, while their velocities are represented as $\dot{\mathbf{s}}_{t,i}=[\dot{x}_{t,i}, \dot{y}_{t,i}, \dot{z}_{t,i}]^T$ and $\dot{\mathbf{s}}_{r,i}=[\dot{x}_{r,i}, \dot{y}_{r,i}, \dot{z}_{r,i}]^T$, for $i=1,2,\ldots, N_t$, $j=1,2,\ldots,N_r$. The target position is represented as $\mathbf{u}=[x^o, y^o, z^o]^T$, with its velocity denoted as $\dot{\mathbf{u}}=[\dot{x}^o, \dot{y}^o, \dot{z}^o]^T$. Each receiver extracts N_t TDs, N_t DSs, and one pair of AOA (an azimuth and an elevation) measurements. These TD-DS-AOA measurements, corresponding to each receiver, are forwarded to the fusion center for centralized localization.

Each receiver measures a pair of AOA (an azimuth $\varphi_j^o \in (-\pi, \pi)$ and an elevation $\theta_j^o \in (0, \pi)$), provided by the following expression:

$$\theta_j^o = \arctan\left(\frac{y^o - y_{r,j}}{x^o - x_{r,j}}\right), \tag{1}$$

$$\varphi_j^o = \arctan\left(\frac{z^o - z_{r,j}}{(x^o - x_{r,j})\cos(\varphi_j^o) + (y^o - y_{r,j})\sin(\varphi_j^o)}\right) \tag{2}$$

where $\arctan(*)$ signifies the inverse tangent function.

By multiplying the TD of the (i,j)th transmitter-receiver pair by the signal propagation speed, we can convert it into the bistatic range (BR). The BR is defined as the sum of transmitter-to-target and target-to-receiver ranges:

$$r_{i,j}^o = R_{t,i}^o + R_{r,j}^o \tag{3}$$

where

$$R_{t,i}^o = \left\|\mathbf{u}^o - \mathbf{s}_{t,i}\right\|, \tag{4}$$

$$R_{r,j}^o = \left\|\mathbf{u}^o - \mathbf{s}_{r,j}\right\|. \tag{5}$$

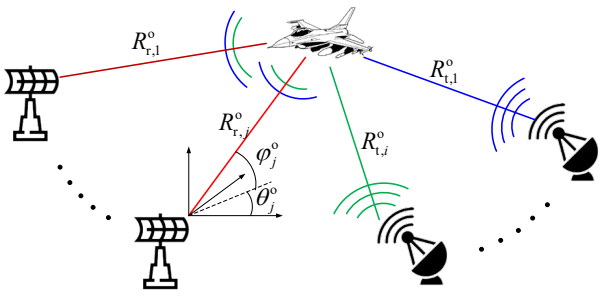

Fig. 1. A typical scenario of multistatic target localization.

Similarly, the DS of the (i, j)th transmitter-receiver pair can be converted into the bistatic range rate (BRR) by multiplying it by the signal wavelength. The BRR is defined as the sum of transmitter-to-target and target-to-receiver range rates, expressed as:

$$\dot{r}_{i,j}^{\mathrm{o}} = \dot{R}_{\mathrm{t},i}^{\mathrm{o}} + \dot{R}_{\mathrm{r},j}^{\mathrm{o}} \tag{6}$$

where

$$\dot{R}_{\mathrm{t},i}^{\mathrm{o}} = \frac{(\mathbf{u}^{\mathrm{o}} - \mathbf{s}_{\mathrm{t},i})^{\mathrm{T}}(\dot{\mathbf{u}}^{\mathrm{o}} - \dot{\mathbf{s}}_{\mathrm{t},i})}{R_{\mathrm{t},i}^{\mathrm{o}}}, \tag{7}$$

$$\dot{R}_{\mathrm{r},j}^{\mathrm{o}} = \frac{(\mathbf{u}^{\mathrm{o}} - \mathbf{s}_{\mathrm{r},j})^{\mathrm{T}}(\dot{\mathbf{u}}^{\mathrm{o}} - \dot{\mathbf{s}}_{\mathrm{r},j})}{R_{\mathrm{r},j}^{\mathrm{o}}}. \tag{8}$$

Given that measurement noise is unavoidable in practical applications, the exact values of azimuth, elevation, BR, and BRR are not directly accessible. Instead, we can only obtain the respective measurements affected by noise:

$$\theta_j = \theta_j^{\mathrm{o}} + \Delta\theta_j, \tag{9}$$

$$\varphi_j = \varphi_j^{\mathrm{o}} + \Delta\varphi_j, \tag{10}$$

$$r_{i,j} = r_{i,j}^{\mathrm{o}} + \Delta r_{i,j}, \tag{11}$$

$$\dot{r}_{i,j} = \dot{r}_{i,j}^{\mathrm{o}} + \Delta\dot{r}_{i,j} \tag{12}$$

where θ_j, φ_j, $r_{i,j}$, and $\dot{r}_{i,j}$ represent the noisy measurements of azimuth, elevation, BR, and BRR, respectively, and $\Delta\theta_j$, $\Delta\varphi_j$, $\Delta r_{i,j}$, and $\Delta\dot{r}_{i,j}$ signify their respective measurement noises. We define the following vectors:

$$\begin{aligned}
&\mathbf{m}_1 = \left[\theta_1, \theta_2, \ldots, \theta_{N_{\mathrm{r}}}\right]^{\mathrm{T}}, \mathbf{m}_2 = \left[\varphi_1, \varphi_2, \ldots, \varphi_{N_{\mathrm{r}}}\right]^{\mathrm{T}}, \\
&\mathbf{m}_3 = \left[\mathbf{r}_1^{\mathrm{T}}, \mathbf{r}_2^{\mathrm{T}}, \ldots, \mathbf{r}_{N_{\mathrm{t}}}^{\mathrm{T}}\right]^{\mathrm{T}}, \mathbf{r}_i = \left[r_{i,1}, r_{i,2}, \ldots, r_{i,N_{\mathrm{r}}}\right]^{\mathrm{T}}, \\
&\mathbf{m}_4 = \left[\dot{\mathbf{r}}_1^{\mathrm{T}}, \dot{\mathbf{r}}_2^{\mathrm{T}}, \ldots, \dot{\mathbf{r}}_{N_{\mathrm{t}}}^{\mathrm{T}}\right]^{\mathrm{T}}, \dot{\mathbf{r}}_i = \left[\dot{r}_{i,1}, \dot{r}_{i,2}, \ldots, \dot{r}_{i,N_{\mathrm{r}}}\right]^{\mathrm{T}},
\end{aligned} \tag{13}$$

$$\begin{aligned}
&\mathbf{m}_1^{\mathrm{o}} = \left[\theta_1, \ldots, \theta_{N_{\mathrm{r}}}^{\mathrm{o}}\right]^{\mathrm{T}}, \mathbf{m}_2^{\mathrm{o}} = \left[\varphi_1^{\mathrm{o}}, \ldots, \varphi_{N_{\mathrm{r}}}^{\mathrm{o}}\right]^{\mathrm{T}}, \\
&\mathbf{m}_3^{\mathrm{o}} = \left[(\mathbf{r}_1^{\mathrm{o}})^{\mathrm{T}}, \ldots, (\mathbf{r}_{N_{\mathrm{t}}}^{\mathrm{o}})^{\mathrm{T}}\right]^{\mathrm{T}}, \mathbf{r}_i^{\mathrm{o}} = \left[r_{i,1}^{\mathrm{o}}, \ldots, r_{i,N_{\mathrm{r}}}^{\mathrm{o}}\right]^{\mathrm{T}}, \\
&\mathbf{m}_4^{\mathrm{o}} = \left[(\dot{\mathbf{r}}_1^{\mathrm{o}})^{\mathrm{T}}, \ldots, (\dot{\mathbf{r}}_{N_{\mathrm{t}}}^{\mathrm{o}})^{\mathrm{T}}\right]^{\mathrm{T}}, \dot{\mathbf{r}}_i^{\mathrm{o}} = \left[\dot{r}_{i,1}^{\mathrm{o}}, \ldots, \dot{r}_{i,N_{\mathrm{r}}}^{\mathrm{o}}\right]^{\mathrm{T}},
\end{aligned} \tag{14}$$

$$\begin{aligned}
&\Delta\mathbf{m}_1 = \left[\Delta\theta_1, \ldots, \Delta\theta_{N_{\mathrm{r}}}\right]^{\mathrm{T}}, \Delta\mathbf{m}_2 = \left[\Delta\varphi_1, \ldots, \Delta\varphi_{N_{\mathrm{r}}}\right]^{\mathrm{T}}, \\
&\Delta\mathbf{m}_3 = \left[\Delta\mathbf{r}_1^{\mathrm{T}}, \ldots, \Delta\mathbf{r}_{N_{\mathrm{t}}}^{\mathrm{T}}\right]^{\mathrm{T}}, \Delta\mathbf{r}_i = \left[\Delta r_{i,1}, \ldots, \Delta r_{i,N_{\mathrm{r}}}\right]^{\mathrm{T}}, \\
&\Delta\mathbf{m}_4 = \left[\Delta\dot{\mathbf{r}}_1^{\mathrm{T}}, \ldots, \Delta\dot{\mathbf{r}}_{N_{\mathrm{t}}}^{\mathrm{T}}\right]^{\mathrm{T}}, \Delta\dot{\mathbf{r}}_i = \left[\Delta\dot{r}_{i,1}, \ldots, \Delta\dot{r}_{i,N_{\mathrm{r}}}\right]^{\mathrm{T}}.
\end{aligned} \tag{15}$$

Without loss of generality, we assume that the azimuth, elevation, BR, and BRR measurement noise vectors independently follow a zero-mean Gaussian distribution with covariance matrices:

$$\mathbf{Q}_1 = \sigma_1^2\mathbf{H}_1, \mathbf{Q}_2 = \sigma_2^2\mathbf{H}_2, \mathbf{Q}_3 = \sigma_3^2\mathbf{H}_3, \mathbf{Q}_4 = \sigma_4^2\mathbf{H}_4 \tag{16}$$

where σ_1^2, σ_2^2, σ_3^2, and σ_4^2 represent the measurement noise powers of azimuth, elevation, BR, and BRR respectively, while $\mathbf{H}_1$, $\mathbf{H}_2$, $\mathbf{H}_3$, and $\mathbf{H}_4$ indicate the structures of the respective covariance matrices $\mathbf{Q}_1$, $\mathbf{Q}_2$, $\mathbf{Q}_3$, and $\mathbf{Q}_4$. Notably, in contrast to previous studies, the measurement noise powers σ_1^2, σ_2^2, σ_3^2, and σ_4^2 are considered unknown.

Subsequently, the azimuth-elevation-BR-BRR measurements can be formulated as vector equations:

$$\mathbf{m} = \mathbf{m}^{\mathrm{o}} + \Delta\mathbf{m} \tag{17}$$

where $\mathbf{m} = [\mathbf{m}_1^{\mathrm{T}}, \mathbf{m}_2^{\mathrm{T}}, \mathbf{m}_3^{\mathrm{T}}, \mathbf{m}_4^{\mathrm{T}}]^{\mathrm{T}}$ symbolizes the vector of azimuth-elevation-BR-BRR measurements, $\mathbf{m}^{\mathrm{o}} = [(\mathbf{m}_1^{\mathrm{o}})^{\mathrm{T}}, (\mathbf{m}_2^{\mathrm{o}})^{\mathrm{T}}, (\mathbf{m}_3^{\mathrm{o}})^{\mathrm{T}}, (\mathbf{m}_4^{\mathrm{o}})^{\mathrm{T}}]^{\mathrm{T}}$ represents the vector of actual azimuth-elevation-BR-BRR values, and $\Delta\mathbf{m} = [\Delta\mathbf{m}_1^{\mathrm{T}}, \Delta\mathbf{m}_2^{\mathrm{T}}, \Delta\mathbf{m}_3^{\mathrm{T}}, \Delta\mathbf{m}_4^{\mathrm{T}}]^{\mathrm{T}}$ represents the vector of azimuth-elevation-BR-BRR measurement noises. This noise vector is a zero-mean Gaussian random vector with the covariance matrix:

$$\mathbf{Q}_{\mathrm{m}} = \mathrm{blkdiag}(\mathbf{Q}_1, \mathbf{Q}_2, \mathbf{Q}_3, \mathbf{Q}_4). \tag{18}$$

This paper considers a localization scenario in which unknown parameters encompass not only the target position $\mathbf{u}^{\mathrm{o}}$ and velocity $\dot{\mathbf{u}}^{\mathrm{o}}$, but also the noise powers σ_1^2, σ_2^2, σ_3^2, and σ_4^2 associated with azimuth-elevation-BR-BRR measurements. Henceforth, the target position and velocity will be collectively referred to as vector $\boldsymbol{\eta}^{\mathrm{o}} = [(\mathbf{u}^{\mathrm{o}})^{\mathrm{T}}, (\dot{\mathbf{u}}^{\mathrm{o}})^{\mathrm{T}}]^{\mathrm{T}}$, and the measurement noise powers will be represented as vector $\boldsymbol{\sigma}^2 = [\sigma_1^2, \sigma_2^2, \sigma_3^2, \sigma_4^2]^{\mathrm{T}}$. The central aim of this paper is to accurately estimate the target position-velocity $\boldsymbol{\eta}^{\mathrm{o}}$, using the azimuth-elevation-BR-BRR measurements $\mathbf{m}$, even when the noise powers $\boldsymbol{\sigma}^2$ remain unknown.

3. Proposed Algorithm

3.1 Maximum Likelihood Estimator

Based on the assumptions previously discussed, we can express the joint conditional probability density function for the azimuth-elevation-BR-BRR measurements as:

$$\begin{aligned}
p(\mathbf{m} \mid \boldsymbol{\eta}^{\mathrm{o}}, \boldsymbol{\sigma}^2) = \prod_{k=1}^{4} &\frac{1}{(2\pi)^{\frac{N_k}{2}} \left(\sigma_k^2\right)^{\frac{N_k}{2}} \left|\mathbf{H}_k\right|^{\frac{1}{2}}} \\
&\times \exp\left[-\frac{(\mathbf{m}_k - \mathbf{m}_k^{\mathrm{o}})^{\mathrm{T}} \mathbf{H}_k^{-1} (\mathbf{m}_k - \mathbf{m}_k^{\mathrm{o}})}{2\sigma_k^2}\right]
\end{aligned} \tag{19}$$

where $N_1 = N_2 = N_{\mathrm{r}}$ and $N_3 = N_4 = N_{\mathrm{t}}N_{\mathrm{r}}$. As a result, the log-likelihood function is represented as:

$$\begin{aligned}
\ln p(\mathbf{m} \mid \boldsymbol{\eta}^{\mathrm{o}}, \boldsymbol{\sigma}^2) = \kappa &- \frac{N_k}{2} \sum_{k=1}^{4} \ln\left(\sigma_k^2\right) \\
&- \frac{1}{2} \sum_{k=1}^{4} \frac{(\mathbf{m}_k - \mathbf{m}_k^{\mathrm{o}})^{\mathrm{T}} \mathbf{H}_k^{-1} (\mathbf{m}_k - \mathbf{m}_k^{\mathrm{o}})}{\sigma_k^2}
\end{aligned} \tag{20}$$

where κ denotes a constant. Consequently, from (20), the MLE for both the target position-velocity and the measurement noise powers can be derived as the following optimization problem:

$$\min_{\boldsymbol{\eta}^{\mathrm{o}},\boldsymbol{\sigma}^2} N_k \sum_{k=1}^{4} \ln\left(\sigma_k^2\right) + \sum_{k=1}^{4} \frac{(\mathbf{m}_k - \mathbf{m}_k^{\mathrm{o}})^{\mathrm{T}} \mathbf{H}_k^{-1} (\mathbf{m}_k - \mathbf{m}_k^{\mathrm{o}})}{\sigma_k^2}. \quad (21)$$

As is evident, the objective function in (21) is both nonconvex and nonlinear. In the subsequent discussion, we will employ a cyclic iteration optimization strategy to minimize the objective function in (21).

3.2 Joint Target Localization and Measurement Noise Power Estimation

The objective function in (21) can be minimized cyclically with respect to $\boldsymbol{\eta}^{\mathrm{o}}$ and $\boldsymbol{\sigma}^2$. More specifically, given an initial estimate for the target position-velocity $\boldsymbol{\eta}$, we derive the partial derivative of (21) with respect to $\boldsymbol{\sigma}^2$ and set it to zero. This yields an estimate of the measurement noise powers as follows:

$$\sigma_k^2 = \frac{(\mathbf{m}_k - \mathbf{m}_k^{\mathrm{o}})^{\mathrm{T}} \mathbf{H}_k^{-1} (\mathbf{m}_k - \mathbf{m}_k^{\mathrm{o}})}{N_k}, k = 1,2,3,4\,. \quad (22)$$

Upon substituting this estimate of $\boldsymbol{\sigma}^2$ into (21), we can derive the update of the target position-velocity estimate via the subsequent minimization:

$$\min_{\boldsymbol{\eta}^{\mathrm{o}}} \sum_{k=1}^{4} \frac{(\mathbf{m}_k - \mathbf{m}_k^{\mathrm{o}})^{\mathrm{T}} \mathbf{H}_k^{-1} (\mathbf{m}_k - \mathbf{m}_k^{\mathrm{o}})}{\sigma_k^2}. \quad (23)$$

Here, we approximate the nonlinear ML problem in (23) as a linear WLS problem. To this end, by applying the tangent function to (1) and (2), we can reformulate the azimuth and elevation equations as:

$$(\boldsymbol{\alpha}_j^{\mathrm{o}})^{\mathrm{T}} \mathbf{u}^{\mathrm{o}} = (\boldsymbol{\alpha}_j^{\mathrm{o}})^{\mathrm{T}} \mathbf{s}_{\mathrm{r},j}^{\mathrm{o}}, \quad (24)$$

$$(\boldsymbol{\beta}_j^{\mathrm{o}})^{\mathrm{T}} \mathbf{u}^{\mathrm{o}} = (\boldsymbol{\beta}_j^{\mathrm{o}})^{\mathrm{T}} \mathbf{s}_{\mathrm{r},j}^{\mathrm{o}} \quad (25)$$

where

$$\boldsymbol{\alpha}_j^{\mathrm{o}} = [\sin(\theta_j^{\mathrm{o}}), -\cos(\theta_j^{\mathrm{o}}), 0]^{\mathrm{T}}, \quad (26)$$

$$\boldsymbol{\beta}_j^{\mathrm{o}} = [\cos(\theta_j^{\mathrm{o}})\sin(\varphi_j^{\mathrm{o}}), \sin(\theta_j^{\mathrm{o}})\sin(\varphi_j^{\mathrm{o}}), -\cos(\varphi_j^{\mathrm{o}})]^{\mathrm{T}}. \quad (27)$$

We can organize (24) corresponding to $j = 1,2,\ldots,N_{\mathrm{r}}$ into vector form as follows:

$$\mathbf{h}_{\theta}^{\mathrm{o}} = \mathbf{G}_{\theta}^{\mathrm{o}} \boldsymbol{\eta}^{\mathrm{o}}, \quad (28)$$

$$\mathbf{h}_{\varphi}^{\mathrm{o}} = \mathbf{G}_{\varphi}^{\mathrm{o}} \boldsymbol{\eta}^{\mathrm{o}} \quad (29)$$

where

$$\left[\mathbf{h}_{\theta}^{\mathrm{o}}\right]_{j,:} = (\boldsymbol{\alpha}_j^{\mathrm{o}})^{\mathrm{T}} \mathbf{s}_{\mathrm{r},j}^{\mathrm{o}}, \left[\mathbf{G}_{\theta}^{\mathrm{o}}\right]_{j,:} = \left[(\boldsymbol{\alpha}_j^{\mathrm{o}})^{\mathrm{T}}, \mathbf{0}_{3\times 1}^{\mathrm{T}}\right], \quad (30)$$

$$\left[\mathbf{h}_{\varphi}^{\mathrm{o}}\right]_{j,:} = (\boldsymbol{\beta}_j^{\mathrm{o}})^{\mathrm{T}} \mathbf{s}_{\mathrm{r},j}^{\mathrm{o}}, \left[\mathbf{G}_{\varphi}^{\mathrm{o}}\right]_{j,:} = \left[(\boldsymbol{\beta}_j^{\mathrm{o}})^{\mathrm{T}}, \mathbf{0}_{3\times 1}^{\mathrm{T}}\right]. \quad (31)$$

To linearize the BR measurements, we rewrite (3) as $r_{i,j}^{\mathrm{o}} - R_{\mathrm{r},j}^{\mathrm{o}} = R_{\mathrm{t},i}^{\mathrm{o}}$ and then square both sides, resulting in:

$$\begin{aligned} 2(\mathbf{s}_{\mathrm{t},i}^{\mathrm{o}} - \mathbf{s}_{\mathrm{r},j}^{\mathrm{o}})^{\mathrm{T}} \mathbf{u}^{\mathrm{o}} - 2r_{i,j}^{\mathrm{o}} R_{\mathrm{r},j}^{\mathrm{o}} &= (\mathbf{s}_{\mathrm{t},i}^{\mathrm{o}})^{\mathrm{T}} \mathbf{s}_{\mathrm{t},i}^{\mathrm{o}} - (\mathbf{s}_{\mathrm{r},j}^{\mathrm{o}})^{\mathrm{T}} \mathbf{s}_{\mathrm{r},j}^{\mathrm{o}} \\ &\quad -(r_{i,j}^{\mathrm{o}})^2. \end{aligned} \quad (32)$$

By defining a unit vector pointing from the jth receiver to the target as follows:

$$\boldsymbol{\rho}_j^{\mathrm{o}} = \left[\cos(\varphi_j^{\mathrm{o}})\cos(\theta_j^{\mathrm{o}}), \cos(\varphi_j^{\mathrm{o}})\sin(\theta_j^{\mathrm{o}}), \sin(\varphi_j^{\mathrm{o}})\right]^{\mathrm{T}} \quad (33)$$

we can derive from the polar coordinates of the target that

$$R_{\mathrm{r},j}^{\mathrm{o}} \boldsymbol{\rho}_j^{\mathrm{o}} = \mathbf{u}^{\mathrm{o}} - \mathbf{s}_{\mathrm{r},j}^{\mathrm{o}}. \quad (34)$$

Premultiplying (34) by $\boldsymbol{\rho}^{\mathrm{o}}_j$ and utilizing the fact $(\boldsymbol{\rho}^{\mathrm{o}}_j)^{\mathrm{T}} \boldsymbol{\rho}^{\mathrm{o}}_j = 1$, we derive:

$$R_{\mathrm{r},j}^{\mathrm{o}} = (\boldsymbol{\rho}_j^{\mathrm{o}})^{\mathrm{T}} (\mathbf{u}^{\mathrm{o}} - \mathbf{s}_{\mathrm{r},j}^{\mathrm{o}}). \quad (35)$$

By substituting (35) into (32), we can deduce that

$$\begin{aligned} 2(\mathbf{s}_{\mathrm{t},i}^{\mathrm{o}} - \mathbf{s}_{\mathrm{r},j}^{\mathrm{o}} - r_{i,j}^{\mathrm{o}} \boldsymbol{\rho}_j^{\mathrm{o}})^{\mathrm{T}} \mathbf{u}^{\mathrm{o}} &= (\mathbf{s}_{\mathrm{t},i}^{\mathrm{o}})^{\mathrm{T}} \mathbf{s}_{\mathrm{t},i}^{\mathrm{o}} - (\mathbf{s}_{\mathrm{r},j}^{\mathrm{o}})^{\mathrm{T}} \mathbf{s}_{\mathrm{r},j}^{\mathrm{o}} \\ &\quad -(r_{i,j}^{\mathrm{o}})^2 - 2r_{i,j}^{\mathrm{o}} (\boldsymbol{\rho}_j^{\mathrm{o}})^{\mathrm{T}} \mathbf{s}_{\mathrm{r},j}^{\mathrm{o}}. \end{aligned} \quad (36)$$

By arranging (36) for $i = 1,2,\ldots,N_{\mathrm{t}}$, $j = 1,2,\ldots,N_{\mathrm{r}}$ in matrix form, we can deduce that:

$$\mathbf{h}_{\mathrm{r}}^{\mathrm{o}} = \mathbf{G}_{\mathrm{r}}^{\mathrm{o}} \boldsymbol{\eta}^{\mathrm{o}} \quad (37)$$

where

$$\begin{aligned} \left[\mathbf{h}_{\mathrm{r}}^{\mathrm{o}}\right]_{(i-1)N_{\mathrm{r}}+j,:} &= (\mathbf{s}_{\mathrm{t},i}^{\mathrm{o}})^{\mathrm{T}} \mathbf{s}_{\mathrm{t},i}^{\mathrm{o}} - (\mathbf{s}_{\mathrm{r},j}^{\mathrm{o}})^{\mathrm{T}} \mathbf{s}_{\mathrm{r},j}^{\mathrm{o}} - (r_{i,j}^{\mathrm{o}})^2 \\ &\quad - 2r_{i,j}^{\mathrm{o}} (\boldsymbol{\rho}_j^{\mathrm{o}})^{\mathrm{T}} \mathbf{s}_{\mathrm{r},j}^{\mathrm{o}}, \\ \left[\mathbf{G}_{\mathrm{r}}^{\mathrm{o}}\right]_{(i-1)N_{\mathrm{r}}+j,:} &= \left[2(\mathbf{s}_{\mathrm{t},i}^{\mathrm{o}} - \mathbf{s}_{\mathrm{r},j}^{\mathrm{o}} - r_{i,j}^{\mathrm{o}} \boldsymbol{\rho}_j^{\mathrm{o}})^{\mathrm{T}}, \mathbf{0}_{3\times 1}^{\mathrm{T}}\right]. \end{aligned} \quad (38)$$

In order to linearize the BRR measurements in (12), we take the derivative of (32) with respect to time, resulting in the following pseudo-linear equation:

$$\begin{aligned} &(\dot{\mathbf{s}}_{\mathrm{t},i}^{\mathrm{o}} - \dot{\mathbf{s}}_{\mathrm{r},j}^{\mathrm{o}})^{\mathrm{T}} \mathbf{u}^{\mathrm{o}} - \dot{r}_{i,j}^{\mathrm{o}} R_{\mathrm{r},j}^{\mathrm{o}} + (\mathbf{s}_{\mathrm{t},i}^{\mathrm{o}} - \mathbf{s}_{\mathrm{r},j}^{\mathrm{o}})^{\mathrm{T}} \dot{\mathbf{u}}^{\mathrm{o}} - r_{i,j}^{\mathrm{o}} \dot{R}_{\mathrm{r},j}^{\mathrm{o}} \\ &= (\mathbf{s}_{\mathrm{t},i}^{\mathrm{o}})^{\mathrm{T}} \dot{\mathbf{s}}_{\mathrm{t},i}^{\mathrm{o}} - (\mathbf{s}_{\mathrm{r},j}^{\mathrm{o}})^{\mathrm{T}} \dot{\mathbf{s}}_{\mathrm{r},j}^{\mathrm{o}} - r_{i,j}^{\mathrm{o}} \dot{r}_{i,j}^{\mathrm{o}}. \end{aligned} \quad (39)$$

Jointly using (8) and (35) yields

$$\dot{R}_{\mathrm{r},j}^{\mathrm{o}} = (\boldsymbol{\rho}_j^{\mathrm{o}})^{\mathrm{T}} (\dot{\mathbf{u}}^{\mathrm{o}} - \dot{\mathbf{s}}_{\mathrm{r},j}^{\mathrm{o}}). \quad (40)$$

Substituting (35) and (40) into (39) yields

$$\begin{aligned} &(\dot{\mathbf{s}}_{\mathrm{t},i}^{\mathrm{o}} - \dot{\mathbf{s}}_{\mathrm{r},j}^{\mathrm{o}} - \dot{r}_{i,j}^{\mathrm{o}} \boldsymbol{\rho}_j^{\mathrm{o}})^{\mathrm{T}} \mathbf{u}^{\mathrm{o}} + (\mathbf{s}_{\mathrm{t},i}^{\mathrm{o}} - \mathbf{s}_{\mathrm{r},j}^{\mathrm{o}} - r_{i,j}^{\mathrm{o}} \boldsymbol{\rho}_j^{\mathrm{o}})^{\mathrm{T}} \dot{\mathbf{u}}^{\mathrm{o}} = (\mathbf{s}_{\mathrm{t},i}^{\mathrm{o}})^{\mathrm{T}} \dot{\mathbf{s}}_{\mathrm{t},i}^{\mathrm{o}} \\ &-(\mathbf{s}_{\mathrm{r},j}^{\mathrm{o}})^{\mathrm{T}} \dot{\mathbf{s}}_{\mathrm{r},j}^{\mathrm{o}} - r_{i,j}^{\mathrm{o}} \dot{r}_{i,j}^{\mathrm{o}} - \dot{r}_{i,j}^{\mathrm{o}} (\boldsymbol{\rho}_j^{\mathrm{o}})^{\mathrm{T}} \mathbf{s}_{\mathrm{r},j}^{\mathrm{o}} - r_{i,j}^{\mathrm{o}} (\boldsymbol{\rho}_j^{\mathrm{o}})^{\mathrm{T}} \dot{\mathbf{s}}_{\mathrm{r},j}^{\mathrm{o}}. \end{aligned} \quad (41)$$

Equation (41) for $i = 1,2,\ldots,N_{\mathrm{t}}$, $j = 1,2,\ldots,N_{\mathrm{r}}$, can be written in matrix form as:

$$\dot{\mathbf{h}}_{\mathrm{r}}^{\mathrm{o}} = \dot{\mathbf{G}}_{\mathrm{r}}^{\mathrm{o}} \boldsymbol{\eta}^{\mathrm{o}} \quad (42)$$

where

$$\begin{aligned} \left[\dot{\mathbf{h}}_{\mathrm{r}}^{\mathrm{o}}\right]_{(i-1)N_{\mathrm{r}}+j,:} &= (\mathbf{s}_{\mathrm{t},i}^{\mathrm{o}})^{\mathrm{T}} \dot{\mathbf{s}}_{\mathrm{t},i}^{\mathrm{o}} - (\mathbf{s}_{\mathrm{r},j}^{\mathrm{o}})^{\mathrm{T}} \dot{\mathbf{s}}_{\mathrm{r},j}^{\mathrm{o}} - r_{i,j}^{\mathrm{o}} \dot{r}_{i,j}^{\mathrm{o}} \\ &\quad - \dot{r}_{i,j}^{\mathrm{o}} (\boldsymbol{\rho}_j^{\mathrm{o}})^{\mathrm{T}} \mathbf{s}_{\mathrm{r},j}^{\mathrm{o}} - r_{i,j}^{\mathrm{o}} (\boldsymbol{\rho}_j^{\mathrm{o}})^{\mathrm{T}} \dot{\mathbf{s}}_{\mathrm{r},j}^{\mathrm{o}}, \\ \left[\dot{\mathbf{G}}_{\mathrm{r}}^{\mathrm{o}}\right]_{(i-1)N_{\mathrm{r}}+j,:} &= \begin{bmatrix} \dot{\mathbf{s}}_{\mathrm{t},i}^{\mathrm{o}} - \dot{\mathbf{s}}_{\mathrm{r},j}^{\mathrm{o}} - \dot{r}_{i,j}^{\mathrm{o}} \boldsymbol{\rho}_j^{\mathrm{o}} \\ \mathbf{s}_{\mathrm{t},i}^{\mathrm{o}} - \mathbf{s}_{\mathrm{r},j}^{\mathrm{o}} - r_{i,j}^{\mathrm{o}} \boldsymbol{\rho}_j^{\mathrm{o}} \end{bmatrix}. \end{aligned} \quad (43)$$

Combining (28), (29), (37), and (42) together, we have

a linear set of azimuth-elevation-BR-BRR equations as follows:

$$\mathbf{h}^{\mathrm{o}} = \mathbf{G}^{\mathrm{o}}\boldsymbol{\eta}^{\mathrm{o}} \tag{44}$$

where

$$\mathbf{h}^{\mathrm{o}} = [(\mathbf{h}_{\theta}^{\mathrm{o}})^{\mathrm{T}}, (\mathbf{h}_{\varphi}^{\mathrm{o}})^{\mathrm{T}}, (\mathbf{h}_{r}^{\mathrm{o}})^{\mathrm{T}}, (\mathbf{h}_{\dot{r}}^{\mathrm{o}})^{\mathrm{T}}]^{\mathrm{T}}, \tag{45}$$

$$\mathbf{G}^{\mathrm{o}} = [(\mathbf{G}_{\theta}^{\mathrm{o}})^{\mathrm{T}}, (\mathbf{G}_{\varphi}^{\mathrm{o}})^{\mathrm{T}}, (\mathbf{G}_{r}^{\mathrm{o}})^{\mathrm{T}}, (\mathbf{G}_{\dot{r}}^{\mathrm{o}})^{\mathrm{T}}]^{\mathrm{T}}. \tag{46}$$

However, in practice, the true azimuth-elevation-BR-BRR values in $\mathbf{h}^{\mathrm{o}}$ and $\mathbf{G}^{\mathrm{o}}$ are not available. To address this, we substitute $\theta_j^{\mathrm{o}} = \theta_j - \Delta\theta_j$, $\varphi_j^{\mathrm{o}} = \varphi_j - \Delta\varphi_j$, $r_{i,j}^{\mathrm{o}} = r_{i,j} - \Delta r_{i,j}$, and $\dot{r}_{i,j}^{\mathrm{o}} = \dot{r}_{i,j} - \Delta\dot{r}_{i,j}$ into (44), and then expand it to the first-order Taylor series, from which can deduce that

$$\mathbf{h} = \mathbf{G}\boldsymbol{\eta}^{\mathrm{o}} + \boldsymbol{\varepsilon} \tag{47}$$

where $\mathbf{h}$ and $\mathbf{G}$ represent the results after replacing the true azimuth-elevation-BR-BRR values with noisy azimuth-elevation-BR-BRR measurements in $\mathbf{h}^{\mathrm{o}}$ and $\mathbf{G}^{\mathrm{o}}$, respectively. $\boldsymbol{\varepsilon}$ denotes the error term, which is associated with the azimuth-elevation-BR-BRR noises as follows:

$$\boldsymbol{\varepsilon} = \mathbf{B}\Delta\mathbf{m} \tag{48}$$

where

$$\mathbf{B} = \begin{bmatrix} \mathbf{B}_{\theta,\theta} & \mathbf{O}_{N_{\mathrm{r}}\times N_{\mathrm{r}}} & \mathbf{O}_{N_{\mathrm{r}}\times N_{\mathrm{t}}N_{\mathrm{r}}} & \mathbf{O}_{N_{\mathrm{r}}\times N_{\mathrm{t}}N_{\mathrm{r}}} \\ \mathbf{B}_{\varphi,\theta} & \mathbf{B}_{\varphi,\varphi} & \mathbf{O}_{N_{\mathrm{r}}\times N_{\mathrm{t}}N_{\mathrm{r}}} & \mathbf{O}_{N_{\mathrm{r}}\times N_{\mathrm{t}}N_{\mathrm{r}}} \\ \mathbf{B}_{r,\theta} & \mathbf{B}_{r,\varphi} & \mathbf{B}_{r,r} & \mathbf{O}_{N_{\mathrm{t}}N_{\mathrm{r}}\times N_{\mathrm{t}}N_{\mathrm{r}}} \\ \mathbf{B}_{\dot{r},\theta} & \mathbf{B}_{\dot{r},\varphi} & \mathbf{B}_{\dot{r},r} & \mathbf{B}_{\dot{r},\dot{r}} \end{bmatrix} \tag{49}$$

with its inner elements given by

$$\begin{aligned}
&[\mathbf{B}_{\theta,\theta}]_{j,j} = \nabla_{\alpha_j,\theta_j}^{\mathrm{T}}(\mathbf{s}_{\mathrm{r},j} - \mathbf{u}^{\mathrm{o}}),\\
&\nabla_{\alpha_j,\theta_j} = [\cos(\theta_j), \sin(\theta_j), 0]^{\mathrm{T}},\\
&[\mathbf{B}_{\varphi,\theta}]_{j,j} = \nabla_{\beta_j,\theta_j}^{\mathrm{T}}(\mathbf{s}_{\mathrm{r},j} - \mathbf{u}^{\mathrm{o}}),\\
&\nabla_{\beta_j,\theta_j} = [-\sin(\varphi_j)\sin(\theta_j), \sin(\varphi_j)\cos(\theta_j), 0]^{\mathrm{T}},\\
&[\mathbf{B}_{\varphi,\varphi}]_{j,j} = \nabla_{\beta_j,\varphi_j}^{\mathrm{T}}(\mathbf{s}_{\mathrm{r},j} - \mathbf{u}^{\mathrm{o}}),\\
&\nabla_{\beta_j,\varphi_j} = [\cos(\varphi_j)\cos(\theta_j), \cos(\varphi_j)\sin(\theta_j), \sin(\varphi_j)]^{\mathrm{T}},\\
&[\mathbf{B}_{r,\theta}]_{(i-1)N_{\mathrm{r}}+j,j} = -2r_{i,j}\nabla_{\rho_j,\theta_j}^{\mathrm{T}}(\mathbf{s}_{\mathrm{r},j} - \mathbf{u}^{\mathrm{o}}),\\
&\nabla_{\rho_j,\theta_j} = [-\cos(\varphi_j)\sin(\theta_j), \cos(\varphi_j)\cos(\theta_j), 0]^{\mathrm{T}},\\
&[\mathbf{B}_{r,\varphi}]_{(i-1)N_{\mathrm{r}}+j,j} = -2r_{i,j}\nabla_{\rho_j,\varphi_j}^{\mathrm{T}}(\mathbf{s}_{\mathrm{r},j} - \mathbf{u}^{\mathrm{o}}),\\
&\nabla_{\rho_j,\varphi_j} = [-\sin(\varphi_j)\cos(\theta_j), -\sin(\varphi_j)\sin(\theta_j), \cos(\varphi_j)]^{\mathrm{T}},\\
&[\mathbf{B}_{r,r}]_{(i-1)N_{\mathrm{r}}+j,(i-1)N_{\mathrm{r}}+j} = -2r_{i,j} - 2\boldsymbol{\rho}_j^{\mathrm{T}}(\mathbf{s}_{\mathrm{r},j} - \mathbf{u}^{\mathrm{o}}),\\
&[\mathbf{B}_{\dot{r},\theta}]_{(i-1)N_{\mathrm{r}}+j,j} = -2\dot{r}_{i,j}\nabla_{\rho_j,\theta_j}^{\mathrm{T}}(\mathbf{s}_{\mathrm{r},j} - \mathbf{u}^{\mathrm{o}}) - 2r_{i,j}\nabla_{\rho_j,\theta_j}^{\mathrm{T}}(\dot{\mathbf{s}}_{\mathrm{r},j} - \dot{\mathbf{u}}^{\mathrm{o}}),\\
&[\mathbf{B}_{\dot{r},\varphi}]_{(i-1)N_{\mathrm{r}}+j,j} = -2\dot{r}_{i,j}\nabla_{\rho_j,\varphi_j}^{\mathrm{T}}(\mathbf{s}_{\mathrm{r},j} - \mathbf{u}^{\mathrm{o}}) - 2r_{i,j}\nabla_{\rho_j,\varphi_j}^{\mathrm{T}}(\dot{\mathbf{s}}_{\mathrm{r},j} - \dot{\mathbf{u}}^{\mathrm{o}}),\\
&[\mathbf{B}_{\dot{r},r}]_{(i-1)N_{\mathrm{r}}+j,(i-1)N_{\mathrm{r}}+j} = -2\dot{r}_{i,j} - 2\boldsymbol{\rho}_j^{\mathrm{T}}(\dot{\mathbf{s}}_{\mathrm{r},j} - \dot{\mathbf{u}}^{\mathrm{o}}),\\
&[\mathbf{B}_{\dot{r},\dot{r}}]_{(i-1)N_{\mathrm{r}}+j,(i-1)N_{\mathrm{r}}+j} = -r_{i,j} - \boldsymbol{\rho}_j^{\mathrm{T}}(\mathbf{s}_{\mathrm{r},j} - \mathbf{u}^{\mathrm{o}})
\end{aligned} \tag{50}$$

for $i = 1,2,\ldots,N_{\mathrm{t}}$, $j = 1,2,\ldots,N_{\mathrm{r}}$, and zeros elsewhere.

From (47) and (48), the azimuth-elevation-BR-BRR measurement noise vector can be approximated as:

$$\Delta\mathbf{m} = \mathbf{B}^{-1}(\mathbf{h} - \mathbf{G}\boldsymbol{\eta}^{\mathrm{o}}). \tag{51}$$

By substituting (50) into (23), the nonlinear ML problem can be derived as the following linear minimization problem:

$$\min_{\boldsymbol{\eta}^{\mathrm{o}}}(\mathbf{h} - \mathbf{G}\boldsymbol{\eta}^{\mathrm{o}})\mathbf{W}(\mathbf{h} - \mathbf{G}\boldsymbol{\eta}^{\mathrm{o}}) \tag{52}$$

where

$$\begin{aligned}
\mathbf{W} &= \mathrm{E}(\boldsymbol{\varepsilon}\boldsymbol{\varepsilon}^{\mathrm{T}})^{-1}\\
&= (\mathbf{B}\mathbf{Q}_{\mathrm{m}}\mathbf{B}^{\mathrm{T}})^{-1}.
\end{aligned} \tag{53}$$

The target position-velocity estimate can be derived from (51) using WLS as:

$$\boldsymbol{\eta} = (\mathbf{G}^{\mathrm{T}}\mathbf{W}\mathbf{G})^{-1}\mathbf{G}^{\mathrm{T}}\mathbf{W}\mathbf{h}. \tag{54}$$

When the measurement noise powers $\boldsymbol{\sigma}^2$ are known, we only need to iteratively compute (52) and (53), thereby minimizing the objective function in (51). However, when given a target position-velocity estimate $\boldsymbol{\eta}$, it is also necessary to iteratively update $\boldsymbol{\sigma}^2$. Thus, in each cycle of iteration, we update the target position-velocity estimate $\boldsymbol{\eta}$ using (52) and (53) once, and then update $\boldsymbol{\sigma}^2$ using (22), and so on.

The implementation of the proposed algorithm is summarized as follows:

Algorithm: Joint Target Localization and Measurement Noise Power Estimation.

Input: azimuth-elevation-BR-BRR measurements $\mathbf{m}$

Output: target position-velocity estimate $\boldsymbol{\eta}$, measurement noise powers $\boldsymbol{\sigma}^2$

Initialize: $t \leftarrow 0$, $\boldsymbol{\eta}^{(0)} = (\mathbf{G}^{\mathrm{T}}\mathbf{G})^{-1}\mathbf{G}^{\mathrm{T}}\mathbf{h}$

Repeat:

Compute $\boldsymbol{\eta}^{(t+1)}$ using (52)

Computing $(\boldsymbol{\sigma}^2)^{(t+1)}$ using (22)

Set $t \leftarrow t+1$

until convergence

Usually, repeating the cycle of iteration two to three times is sufficient to yield an estimate reaching the CRLB accuracy. More repetitions will not enhance accuracy nor degrade it.

4. CRLB Analysis

In this section, we derive the CRLB for the proposed algorithm, a theoretical lower error bound commonly used for any unbiased estimate of deterministic parameters. For the localization issue described in this paper, the unknown

parameters include the target position-velocity $\boldsymbol{\eta}^{\mathrm{o}}$ and the measurement noise powers $\boldsymbol{\sigma}^2$, combined here as a vector $\boldsymbol{\psi} = [(\boldsymbol{\eta}^{\mathrm{o}})^{\mathrm{T}}, \boldsymbol{\sigma}^2]^{\mathrm{T}}$.

Invoking the definition, we have the CRLB for $\boldsymbol{\psi}$ as follows

$$\mathrm{CRLB}(\boldsymbol{\psi}) = \mathrm{FIM}(\boldsymbol{\psi})^{-1} \tag{55}$$

where $\mathrm{FIM}(\boldsymbol{\psi})$ denotes Fisher's information matrix (FIM) defined as:

$$\mathrm{FIM}(\boldsymbol{\psi}) = \mathrm{E}\left[\left(\frac{\partial \ln p(\mathbf{m}\,|\,\boldsymbol{\psi})}{\partial \boldsymbol{\psi}}\right)^{\mathrm{T}}\left(\frac{\partial \ln p(\mathbf{m}\,|\,\boldsymbol{\psi})}{\partial \boldsymbol{\psi}}\right)\right]. \tag{56}$$

Substitute (20) into (54) and use the following statistical properties of a Gaussian variable:

$$\mathrm{E}(x) = 0, \mathrm{E}(x^2) = 1, \mathrm{E}(x^3) = 0, \mathrm{E}(x^4) = 3 \tag{57}$$

which can deduce, after some algebraic manipulations, the CRLB of the target position-velocity $\boldsymbol{\eta}^{\mathrm{o}}$ and the measurement noise powers $\boldsymbol{\sigma}^2$ as:

$$\mathrm{CRLB}(\boldsymbol{\eta}^{\mathrm{o}}) = \left(\frac{\partial \mathbf{m}^{\mathrm{o}}}{\partial \boldsymbol{\eta}^{\mathrm{o}}}\right)^{\mathrm{T}} \mathbf{Q}^{-1} \frac{\partial \mathbf{m}^{\mathrm{o}}}{\partial \boldsymbol{\eta}^{\mathrm{o}}}, \tag{58}$$

$$\mathrm{CRLB}(\boldsymbol{\sigma}^2) = 2\,\mathrm{diag}\left\{\frac{\sigma_1^4}{N_1}, \frac{\sigma_2^4}{N_2}, \frac{\sigma_3^4}{N_3}, \frac{\sigma_4^4}{N_4}\right\} \tag{59}$$

where $\partial \mathbf{m}^{\mathrm{o}} / \partial \boldsymbol{\eta}^{\mathrm{o}}$ can be derived as:

$$\frac{\partial \mathbf{m}^{\mathrm{o}}}{\partial \boldsymbol{\eta}^{\mathrm{o}}} = \begin{bmatrix} \dfrac{\partial \mathbf{m}_1^{\mathrm{o}}}{\partial \mathbf{u}^{\mathrm{o}}} & \mathbf{O}_{N_{\mathrm{r}} \times 3} \\ \dfrac{\partial \mathbf{m}_2^{\mathrm{o}}}{\partial \mathbf{u}^{\mathrm{o}}} & \mathbf{O}_{N_{\mathrm{r}} \times 3} \\ \dfrac{\partial \mathbf{m}_3^{\mathrm{o}}}{\partial \mathbf{u}^{\mathrm{o}}} & \mathbf{O}_{N_{\mathrm{t}} N_{\mathrm{r}} \times 3} \\ \dfrac{\partial \mathbf{m}_4^{\mathrm{o}}}{\partial \mathbf{u}^{\mathrm{o}}} & \dfrac{\partial \mathbf{m}_4^{\mathrm{o}}}{\partial \dot{\mathbf{u}}^{\mathrm{o}}} \end{bmatrix} \tag{60}$$

with

$$\left[\frac{\partial \mathbf{m}_1^{\mathrm{o}}}{\partial \mathbf{u}^{\mathrm{o}}}\right]_{j,:} = \begin{bmatrix} \dfrac{-(y^{\mathrm{o}} - y_{\mathrm{r},j}^{\mathrm{o}})}{(x^{\mathrm{o}} - x_{\mathrm{r},j}^{\mathrm{o}})^2 + (y^{\mathrm{o}} - y_{\mathrm{r},j}^{\mathrm{o}})^2} \\ \dfrac{(x^{\mathrm{o}} - x_{\mathrm{r},j}^{\mathrm{o}})}{(x^{\mathrm{o}} - x_{\mathrm{r},j}^{\mathrm{o}})^2 + (y^{\mathrm{o}} - y_{\mathrm{r},j}^{\mathrm{o}})^2} \\ 0 \end{bmatrix},$$

$$\left[\frac{\partial \mathbf{m}_2^{\mathrm{o}}}{\partial \mathbf{u}^{\mathrm{o}}}\right]_{j,:} = \begin{bmatrix} \dfrac{-(x^{\mathrm{o}} - x_{\mathrm{r},j}^{\mathrm{o}})(z^{\mathrm{o}} - z_{\mathrm{r},j}^{\mathrm{o}})}{(R_{\mathrm{r},j}^{\mathrm{o}})^2 \sqrt{(x^{\mathrm{o}} - x_{\mathrm{r},j}^{\mathrm{o}})^2 + (y^{\mathrm{o}} - y_{\mathrm{r},j}^{\mathrm{o}})^2}} \\ \dfrac{-(y^{\mathrm{o}} - y_{\mathrm{r},j}^{\mathrm{o}})(z^{\mathrm{o}} - z_{\mathrm{r},j}^{\mathrm{o}})}{(R_{\mathrm{r},j}^{\mathrm{o}})^2 \sqrt{(x^{\mathrm{o}} - x_{\mathrm{r},j}^{\mathrm{o}})^2 + (y^{\mathrm{o}} - y_{\mathrm{r},j}^{\mathrm{o}})^2}} \\ \dfrac{\sqrt{(x^{\mathrm{o}} - x_{\mathrm{r},j}^{\mathrm{o}})^2 + (y^{\mathrm{o}} - y_{\mathrm{r},j}^{\mathrm{o}})^2}}{(R_{\mathrm{r},j}^{\mathrm{o}})^2} \end{bmatrix},$$

$$\left[\frac{\partial \mathbf{m}_3^{\mathrm{o}}}{\partial \mathbf{u}^{\mathrm{o}}}\right]_{(i-1)N_{\mathrm{r}}+j,:} = \frac{(\mathbf{u}^{\mathrm{o}} - \mathbf{s}_{\mathrm{t},i}^{\mathrm{o}})^{\mathrm{T}}}{R_{\mathrm{t},i}^{\mathrm{o}}} + \frac{(\mathbf{u}^{\mathrm{o}} - \mathbf{s}_{\mathrm{r},j}^{\mathrm{o}})^{\mathrm{T}}}{R_{\mathrm{r},j}^{\mathrm{o}}},$$

$$\left[\frac{\partial \mathbf{m}_4^{\mathrm{o}}}{\partial \mathbf{u}^{\mathrm{o}}}\right]_{(i-1)N_{\mathrm{r}}+j,:} = \frac{(\dot{\mathbf{u}}^{\mathrm{o}} - \dot{\mathbf{s}}_{\mathrm{t},i}^{\mathrm{o}})^{\mathrm{T}} R_{\mathrm{t},i}^{\mathrm{o}} - (\mathbf{u}^{\mathrm{o}} - \mathbf{s}_{\mathrm{t},i}^{\mathrm{o}})^{\mathrm{T}} \dot{R}_{\mathrm{t},i}^{\mathrm{o}}}{(R_{\mathrm{t},i}^{\mathrm{o}})^2} + \frac{(\dot{\mathbf{u}}^{\mathrm{o}} - \dot{\mathbf{s}}_{\mathrm{r},j}^{\mathrm{o}})^{\mathrm{T}} R_{\mathrm{r},j}^{\mathrm{o}} - (\mathbf{u}^{\mathrm{o}} - \mathbf{s}_{\mathrm{r},j}^{\mathrm{o}})^{\mathrm{T}} \dot{R}_{\mathrm{r},j}^{\mathrm{o}}}{(R_{\mathrm{r},j}^{\mathrm{o}})^2}, \tag{61}$$

$$\left[\frac{\partial \mathbf{m}_4^{\mathrm{o}}}{\partial \dot{\mathbf{u}}^{\mathrm{o}}}\right]_{(i-1)N_{\mathrm{r}}+j,:} = \frac{(\mathbf{u}^{\mathrm{o}} - \mathbf{s}_{\mathrm{t},i}^{\mathrm{o}})^{\mathrm{T}}}{R_{\mathrm{t},i}^{\mathrm{o}}} + \frac{(\mathbf{u}^{\mathrm{o}} - \mathbf{s}_{\mathrm{r},j}^{\mathrm{o}})^{\mathrm{T}}}{R_{\mathrm{r},j}^{\mathrm{o}}}.$$

5. Simulation and Discussions

In this section, we assess the localization performance of the proposed algorithm through numerical simulations. We measure the localization performance by the root mean square error (RMSE) of the target position-velocity and the measured noise powers, calculated as:

$$\mathrm{RMSE}(\mathbf{u}) = \sqrt{\frac{1}{L}\sum_{l=1}^{L}\left\|\mathbf{u}^{(l)} - \mathbf{u}^{\mathrm{o}}\right\|^2},$$

$$\mathrm{RMSE}(\dot{\mathbf{u}}) = \sqrt{\frac{1}{L}\sum_{l=1}^{L}\left\|\dot{\mathbf{u}}^{(l)} - \dot{\mathbf{u}}^{\mathrm{o}}\right\|^2}, \tag{62}$$

$$\mathrm{RMSE}(\sigma_k^2) = \sqrt{\frac{1}{L}\sum_{l=1}^{L}\left(\sigma_k^{2(l)} - \sigma_k^2\right)^2}, k = 1,2,3,4$$

where $\mathbf{u}^{(l)}$, $\dot{\mathbf{u}}^{(l)}$, and $\sigma_k^{2(l)}$ are estimates of $\mathbf{u}^{\mathrm{o}}$, $\dot{\mathbf{u}}^{\mathrm{o}}$, and σ_k^2 at the lth run, respectively, and $L = 1000$ is the total number of simulation runs. The simulation scenario is illustrated in Fig. 2.

As depicted in Fig. 2, we consider a multistatic localization system with $N_{\mathrm{t}} = 4$ transmitters and $N_{\mathrm{r}} = 5$ receivers. Their positions and velocities are listed in Tab. 1. The R value is the radius of the circle in which the transmitters/receivers are located in Fig. 2, and in this case, it is measured as $R = 1000$ m. The azimuth, elevation, BR, and BRR measurement noise covariances are set to:

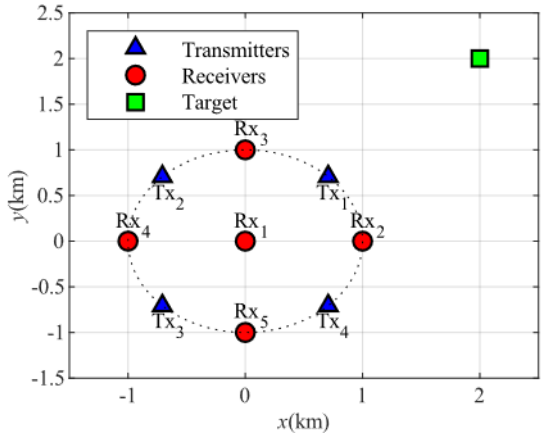

Fig. 2. Localization geometry.

Tx no. i	$x_{t,i}$ (m)	$y_{t,i}$ (m)	$z_{t,i}$ (m)	$\dot{x}_{t,i}$ (m/s)	$\dot{y}_{t,i}$ (m/s)	$\dot{z}_{t,i}$ (m/s)
1	R cos(45°)	R sin(45°)	300	10	10	10
2	R cos(135°)	R sin(135°)	250	20	0	0
3	R cos(225°)	R sin(225°)	400	10	100	10
4	R cos(315°)	R sin(315°)	100	20	15	10
Rx no. j	$x_{r,j}$ (m)	$y_{r,j}$ (m)	$z_{r,j}$ (m)	$\dot{x}_{r,j}$ (m/s)	$\dot{y}_{r,j}$ (m/s)	$\dot{z}_{r,j}$ (m/s)
1	0	0	100	30	–20	20
2	R cos(0°)	R sin(0°)	200	–30	10	20
3	R cos(90°)	R sin(90°)	350	10	–20	10
4	R cos(180°)	R sin(180°)	250	10	20	30
5	R cos(270°)	R sin(270°)	400	–20	10	10

Tab. 1. Positions and velocities of transmitters and receivers.

$\mathbf{Q}_1 = \sigma_1^2\mathbf{I}_{N_tN_r}$, $\mathbf{Q}_2 = \sigma_2^2\mathbf{I}_{N_tN_r}$, $\mathbf{Q}_3 = \sigma_3^2\mathbf{I}_{N_t}$, $\mathbf{Q}_4 = \sigma_4^2\mathbf{I}_{N_r}$, where the measurement noise standard deviations σ_1, σ_2, σ_3, and σ_4 are set to $\sigma_1 = 0.1\ \sigma_m$ (deg), $\sigma_2 = 0.1\ \sigma_m$ (deg), $\sigma_3 = \sigma_m$ (m), and $\sigma_1 = 0.01\ \sigma_m$ (m/s), respectively, with σ_m controlling the overall measurement noise level in the simulations.

5.1 Convergence of the Algorithm

To visualize the convergence process of our proposed algorithm, we plot the target position-velocity estimate and the corresponding objective function versus the number of iterations during the calculation process. Here, one iteration signifies one update of the target position-velocity estimate $\boldsymbol{\eta}$ and the measurement noise power $\boldsymbol{\sigma}^2$. The simulation results are depicted in Fig. 3 and Fig. 4.

As depicted in Fig. 3, it is evident that the localization results produced by the proposed algorithm rapidly reduce the objective function as the number of iterations increases. Upon conducting multiple simulations, we generally found that the objective function converges to a sufficiently small value and remains practically unchanged after 2 to 3 iterations. Thus, increasing the number of iterations at this stage would not enhance the target localization accuracy, but would instead add to the time cost. Additionally, as indicated in Fig. 4, the WLS solution used by the proposed algorithm for the initial iteration is positioned close to the true location of the target, ensuring quick convergence of the iterations to the true location of the target.

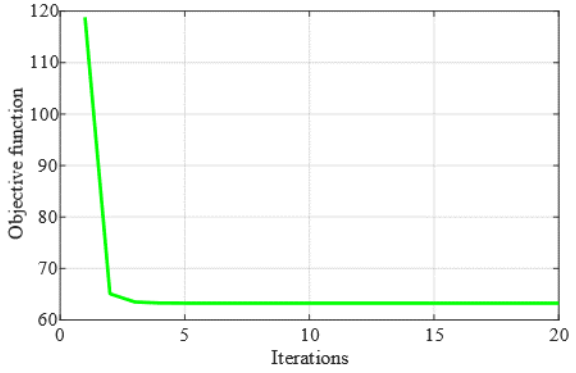

Fig. 3. Variation of the objective function with the number of iterations.

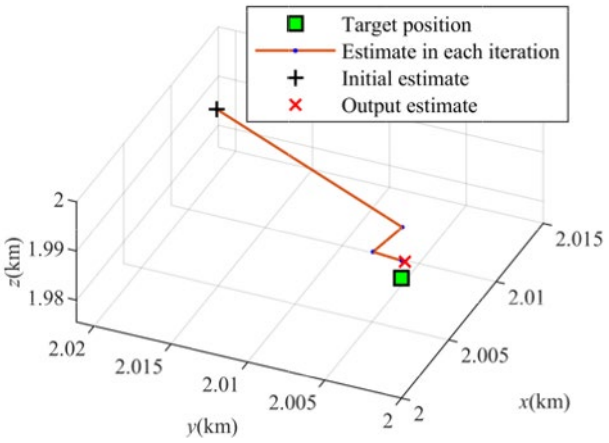

Fig. 4. Variation of the target position estimate with the number of iterations.

5.2 Localization RMSE of the Algorithm at Different Measurement Noise Levels

We now compare the localization RMSE of the proposed algorithm with existing algorithms, as well as with the CRLB. The benchmark algorithms include those developed in references [18], [20], and [21], conveniently abbreviated as mWLS-Li, mWLS-Yang, and 1WLS-Wei, respectively. The overall measurement noise level is set between –10 dB to 50 dB. As mentioned earlier, the implementations of mWLS-Li, mWLS-Yang, and 1WLS-Wei algorithms require the measurement noise powers. This paper considers a more practical non-ideal localization scenario, where the measurement noise powers are assumed unknown. In this section, we proceed to evaluate the localization performance of the algorithms in this non-ideal scenario, hence the measurement noise powers are not available. In this case, the measurement noise powers can be artificially specified to certain values. Obviously, the values of the measurement noise powers have a significant impact on the algorithm performance; the closer they are to the true measurement noise powers, the better the localization performance, and vice versa. In order to compare the simulation performance fairly, we set the measurement noise powers to be randomly distributed within their range of values, in order to minimize the effect of subjective settings on the simulation results. The estimation RMSEs of the algorithms on target position and velocity are plotted in Fig. 5.

The RMSEs of the algorithms for target position-velocity estimation at measurement noise levels from –10 dB to 40 dB are provided in Fig. 5. It is observed that when the measurement noise powers are unknown, the localization RMSEs of mWLS-Li, mWLS-Yang, and 1WLS-Wei algorithms do not reach the CRLB at different measurement noise levels. Contrastingly, the localization RMSE of our proposed algorithm is significantly lower and approximates the CRLB at mild measurement noise levels ($20\ \lg(\sigma_m) \le 40$ dB). Due to the nonlinearity of the localization issue, the target position-velocity RMSE curves of

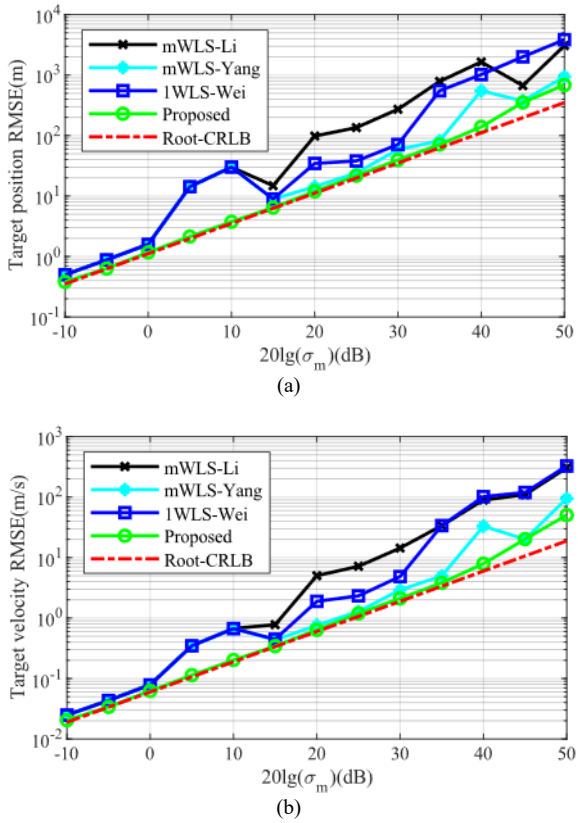

Fig. 5. Localization RMSE of the algorithms at different measurement noise levels. (a) Target position estimation. (b) Target velocity estimation.

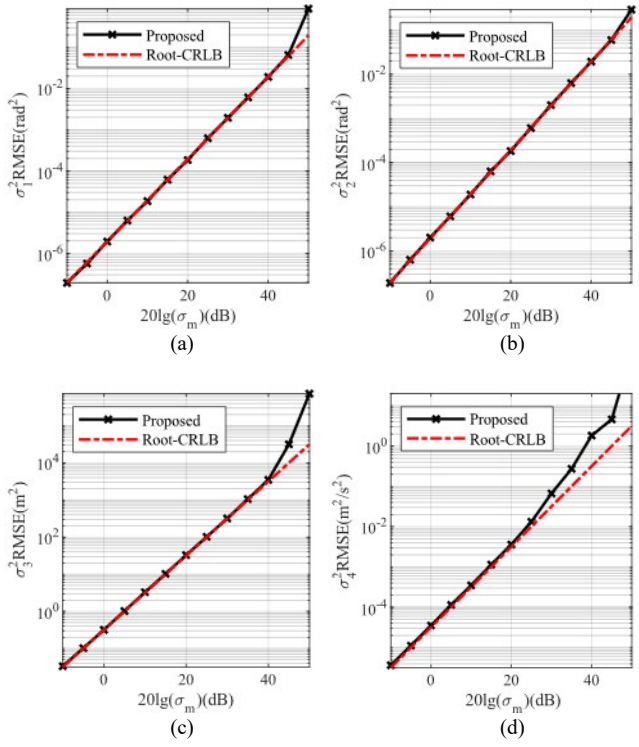

Fig. 6. Estimation performance of the measurement noise powers. (a) Azimuth measurement noise power estimation. (b) Elevation measurement noise power estimation. (c) BR measurement noise power estimation. (d) BRR measurement noise power estimation.

the proposed algorithm slightly deviate from the CRLB at large measurement noise levels ($20\lg(\sigma_m) > 40$ dB). However, the localization RMSE of the proposed algorithm is about an order of magnitude smaller than that of existing algorithms.

While the proposed algorithm estimates the target position and velocity, it also estimates the measurement noise powers. The corresponding simulation results are illustrated in Fig. 6.

As existing algorithms fail to estimate the measurement noise powers, Figure 6 includes only the RMSEs of the measurement noise powers estimated by the proposed algorithm. The RMSEs of the estimated measurement noise powers by the proposed algorithm approximate the CRLB at measurement noise levels of $20\lg(\sigma_m) < 40$ dB. As anticipated, the RMSE curves deviate from the CRLB under large measurement noise conditions of $20\lg(\sigma_m) > 40$ dB. This is mainly due to the higher-order error terms discarded by the proposed algorithm when linearizing the azimuth, elevation, BR, and BRR measurement equations. Note that Figure 6(d) is different form remaining sub-plots, the RMSE curve of σ_4 deviating from the CRLB at a threshold of 30 dB, about 10 dB smaller than other sub-plots. This is because the relative value of the BRR measurement noise power σ_4 to the overall measurement error power σ_m is smaller than that of the other measurement noise powers σ_1, σ_2, σ_3, which causes the RMSE of σ_4 to deviate more easily from the CRLB compared to σ_1, σ_2, σ_3.

5.3 CDOP Analysis

Sections 5.1 and 5.2 analyze the localization performance of the algorithm for only one transmitter/receiver geometry. To further explore the impact of different transmitter/receiver geometries on the localization accuracy, we introduce here the Geometric Dilution Of Precision (GDOP) factor for target localization. The GDOP plot shows the localization accuracy achievable with a particular geometry of the MIMO radar, where the color bar represents the normalized localization error. Lower values indicate that the geometry provides higher localization accuracy.

Figure 7 shows the GDOP contour plots for target localization by the distributed MIMO radar with symmetric and asymmetric geometries for a measurement noise level of $20\lg(\sigma_m) = 30$ dB and a target height of $z = 0.5R$ and $z = 5R$. It can be found that the localization accuracy decreases for targets farther away from the central coverage area where the distributed MIMO radar is located. Moreover, the target localization accuracy is highest at the location of the MIMO radar area. Comparing the contours in Fig. 7(a) and (b) shows that the distance of the target from the center region has less effect on the target localization accuracy when the target height is higher. Comparing the contours in Fig. 7(a) and (c) shows that the MIMO radar with symmetric geometry has better localization performance compared to the MIMO radar with asymmetric geometry.

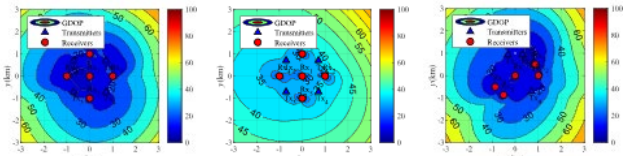

(a) (b) (c)

Fig. 7. GDOP plot for different geometries. (a) Symmetrical geometry, $z = 0.5R$. (b) Symmetrical geometry, $z = 5R$. (c) Asymmetric geometry, $z = 0.5R$.

Algorithm	Average Computational Time (ms)
mWLS-Li	1.410130
mWLS-Yang	0.942750
1WLS-Wei	1.112495
Proposed	2.812392

Tab. 2. Average computational time of the algorithms.

5.4 Comparison of Computation Efficiency

Finally, we conduct simulations using the algorithms on the same computer and calculate the average time required for a single run of the algorithms to quantitatively evaluate their computational complexity. The main specifications of the computer are as follows: CPU: Intel(R) Core(TM) i7-8550U @1.80 GHz; RAM: 16 GB DDR4 2666 MHz; Operating system: Windows 10; Software: MATLAB R2021b. The simulation results are displayed in Tab. 2.

As evident in Tab. 2, the average computational time of the proposed algorithm is 1.4 ms, 1.9 ms and 1.7 ms higher than that of the mWLS-Li, mWLS-Yang, and 1WLS-Wei algorithms. This is owing to the additional computation required for measuring noise powers during the iteration. However, since the proposed algorithm only requires two to three iterations to converge, compared to the mWLS-Li, mWLS-Yang, and 1WLS-Wei algorithms, the computational time of the proposed algorithm is of the same order of magnitude as that of the existing algorithms. Moreover, considering that the proposed algorithm does not necessitate prior knowledge of the measurement noise powers while maintaining solid localization performance, the slight increase in computational time is acceptable.

6. Conclusion

In this paper, we have investigated the multistatic target localization issue with AOA, TD, and DS measurements under conditions of unknown measurement noise powers. We have proposed a joint target localization and measurement noise power estimation algorithm based on cyclical iterations. Compared with existing algorithms, the proposed algorithm does not require any prior knowledge of the measurement noise powers and can estimate both the target position-velocity and the measurement noise powers, making it more versatile in practice. Simulation results demonstrate that the proposed algorithm has superior localization accuracy compared to existing algorithms under conditions of unknown measurement noise powers, and can approximate the CRLB at mild measurement noise levels. The instability of the proposed algorithm at large measurement noise levels has been found through the simulation and theoretical analysis. In our further study, we will take this issue as the key point and find an improved method to avoid this problem.

References

[1] DONTAMSETTI, S. G., KUMAR, R. V. R. A distributed MIMO radar with joint optimal transmit and receive signal combining. *IEEE Transactions on Aerospace and Electronic Systems*, 2021, vol. 57, no. 1, p. 623–635. DOI: 10.1109/TAES.2020.3027103

[2] ZAIMBASHI, A. A unified framework for multistatic passive radar target detection under uncalibrated receivers. *IEEE Transactions on Signal Processing*, 2021, vol. 69, p. 695–708. DOI: 10.1109/TSP.2020.3048800

[3] FUGENSCHUH, A. R., CRAPARO, E. M., KARATAS, M., et al. Solving multistatic sonar location problems with mixed-integer programming. *Optimization and Engineering*, 2019, vol. 21, p. 273–303. DOI: 10.1007/s11081-019-09445-2

[4] SAHR, J. D., LIND, F. D. The Manastash Ridge radar: A passive bistatic radar for upper atmospheric radio science. *Radio Science*, 1997, vol. 32, no. 6, p. 2345–2358. DOI: 10.1029/97RS02454

[5] NOROOZI, A., SEBT, M. A. Target localization in multistatic passive radar using SVD approach for eliminating the nuisance parameters. *IEEE Transactions on Aerospace & Electronic Systems*, 2017, vol. 53, no. 4, p. 1660–1671. DOI: 10.1109/TAES.2017.2669558

[6] AMIRI, R., BEHNIA, F., ZAMANI, H. Asymptotically efficient target localization from bistatic range measurements in distributed MIMO radars. *IEEE Signal Processing Letters*, 2017, vol. 24, no. 3, p. 299–303. DOI: 10.1109/LSP.2017.2660545

[7] AMIRI, R., BEHNIA, F., SADR, M. A. M. Exact solution for elliptic localization in distributed MIMO radar systems. *IEEE Transactions on Vehicular Technology*, 2018, vol. 67, no. 2, p. 1075–1086. DOI: 10.1109/TVT.2017.2762631

[8] PANWAR, K., BABU, P., STOICA, P. Maximum likelihood algorithm for time-delay based multistatic target localization. *IEEE Signal Processing Letters*, 2022, vol. 29, p. 847–851. DOI: 10.1109/LSP.2022.3158592

[9] NOROOZI, A., SEBT, M. A. Algebraic solution for three-dimensional TDOA/AOA localisation in multiple-input–multiple-output passive radar. *IET Radar, Sonar & Navigation*, 2018, vol. 12, no. 1, p. 21–29. DOI: 10.1049/iet-rsn.2017.0117

[10] AMIRI, R., BEHNIA, F., ZAMANI, H. Efficient 3-D positioning using time-delay and AOA measurements in MIMO radar systems. *IEEE Communications Letters*, 2017, vol. 21, no. 12, p. 2614 to 2617. DOI: 10.1109/LCOMM.2017.2742945

[11] KAZEMI, S. A. R., AMIRI, R., BEHNIA, F. Efficient closed-form solution for 3-D hybrid localization in multistatic radars. *IEEE Transactions on Aerospace and Electronic Systems*, 2021, vol. 57, no. 6, p. 3886–3895. DOI: 10.1109/TAES.2021.3082664

[12] LIU, M. M., GAO, W., ZHAO, Y. An efficient estimator for source localization using TD and AOA measurements in MIMO radar systems. *IEEE Sensors Letters*, 2021, vol. 5, no. 3, p. 1–4. DOI: 10.1109/LSENS.2021.3057363

[13] KAZEMI, S. A. R., AMIRI, R., BEHNIA, F. Efficient convex solution for 3-D localization in MIMO radars using delay and angle measurements. *IEEE Communications Letters*, 2019, vol. 23, no. 12, p. 2219–2223. DOI: 10.1109/LCOMM.2019.2948175

[14] ZHU, L., WE, G., SONG, H., et al. Robust moving target localization in distributed MIMO radars via iterative Lagrange programming neural network. *IEEE Sensors Journal*, 2020, vol. 20, no. 21, p. 13007–13017. DOI: 10.1109/JSEN.2020.3003349

[15] NOROOZI, A., AMIRI, R., NAYEBI, M. M., et al. Efficient closed-form solution for moving target localization in MIMO radars with minimum number of antennas. *IEEE Transactions on Signal Processing*, 2020, vol. 68, p. 2545–2557. DOI: 10.1109/TSP.2020.2986163

[16] ZHANG, F., SUN, Y., ZOU, J., et al. Closed-form localization method for moving target in passive multistatic radar network. *IEEE Sensors Journal*, 2020, vol. 20, no. 2, p. 980–990. DOI: 10.1109/JSEN.2019.2944957

[17] SONG, H., WEN, G., ZHU, L. An approximately efficient estimator for moving target localization in distributed MIMO radar systems in presence of sensor location errors. *IEEE Sensors Journal*, 2020, vol. 20, no. 2, p. 931–938. DOI: 10.1109/JSEN.2019.2943738

[18] KAZEMI, S. A. R., AMIRI, R., BEHNIA, F. An approximate ML estimator for moving target localization in distributed MIMO radars. *IEEE Signal Processing Letters*, 2020, vol. 27, p. 1595 to 1599. DOI: 10.1109/LSP.2020.3020505

[19] ZHAO, Y., ZHAO, C., LIANG, J. New algebraic algorithm for moving target localization in distributed MIMO radar systems. *Journal of Electronics & Information Technology*, 2018, vol. 40, no. 3, p. 548–556. DOI: 10.11999/JEIT170510

[20] JABBARI, M. R., TABAN, M. R., GAZOR, S. A robust TSWLS localization of moving target in widely separated MIMO radars. *IEEE Transactions on Aerospace and Electronic Systems*, 2023, vol. 59, no. 2, p. 897–906. DOI: 10.1109/TAES.2022.3194112

[21] LI, W., TANG, Q., HUANG, C., et al. Location algorithms for moving target in non-coherent distributed multiple-input multiple-output radar systems. *IET Signal Processing*, 2017, vol. 11, no. 5, p. 503–514. DOI: 10.1049/iet-spr.2016.0323

[22] CHAN, Y. T., HO, K. C. A simple and efficient estimator for hyperbolic location. *IEEE Transactions on Signal Processing*, 1994, vol. 42, no. 8, p. 1905–1915. DOI: 10.1109/78.301830

[23] YANG, L., YANG, L., HO, K. C. Moving target localization in multistatic sonar using time delays, Doppler shifts and arrival angles. In *IEEE International Conference on Acoustics, Speech and Signal Processing (ICASSP)*. New Orleans (LA, USA), 2017, p. 3399–3403. DOI: 10.1109/ICASSP.2017.7952787

[24] WEI, Y., LI, W., TANG, Q., et al. A closed-form location algorithm without auxiliary variables for moving target in noncoherent multiple-input and multiple-output radar system. *IEEE Access*, 2020, vol. 8, p. 69496–69508. DOI: 10.1109/ACCESS.2020.2984825

About the Authors …

Jing YANG was born in 1985. She received her M.Sc. from the National Digital Switching System Engineering and Technological Research Center in 2011. Her research interests include target location, parameter estimation, and target detection of passive radar.

Chengcheng LIU (corresponding author) was born in 1986. He received his Ph.D. from the National Digital Switching System Engineering and Technological Research Center in 2014. His research interests include wideband array signal processing.

Jie HUANG was born in 1973. She received her Ph.D. from the National Digital Switching System Engineering and Technological Research Center in 2017. Her research interests include target detection and acquisition.

Dexiu HU was born in 1983. He received his Ph.D. from Tsinghua University in 2017. His research interests include electron reconnaissance.

Chuang ZHAO was born in 1978. He received his Ph.D. from the National Digital Switching System Engineering and Technological Research Center in 2019. His research interests include electron reconnaissance.